Interreg North-West Europe RAWFILL

European Regional Development Fund

Co-funded by the Walloon region

DI2.2.3 Deliverable – Geophysical imaging post-sampling report

Date: January, 2020

SPAQuE.be

SAMEN MAKEN WE MORGEN MOOIER OVAM

LIÈGE université

BGS 1835 British Geological Survey Expert | Impartial | Innovative

atrasol SUSTAINABLE CONSULTANT

BAV Bergischer Abfallwirtschaftsverband

LES CHAMPS JOUAULT

Cleantech Flanders Powered by VITO

SUBJECT:	Geophysical imaging post-sampling report						
☒	report	☐	information	☐	consideration	☐	decision
To:	…			From:	Liège and BGS		

Introduction

The following report describes the results of the post-sampling geophysical survey carried out on the landfill of Les Champs Jouault (France), the second pilot site of the RAWFILL project. The purpose of the survey is to refine the geophysical images obtained during the first geophysical survey (see Deliverable I2.2.2) and improve correlations with the sampling results.

The described investigations were conducted in November 25th – 27th 2019. They were prepared in close coordination with SAS Les Champs Jouault, partner of the RAWFILL project. Geophysical measurements were taken just before the sampling begun to ensure that the surveyed areas were not too overly disturbed.

Summary of the study area and previous investigations

The landfill of Les Champs Jouault, in activity since 2009, contains mainly municipal and industrial solid waste (MSW and ISW) in almost equal proportion. More information about the site can be found in Deliverable I2.1.1. During the first geophysical survey (see Deliverable I2.2.2), four cells were investigated (see Fig. 1). Based on the results obtained, a sampling plan consisting of three boreholes and two 15m long trenches was proposed (see Deliverable I2.3.1 and Fig. 2). Due to the presence of buried gas extraction/leachate injection pipes and buried monitoring devices, not all anomalous zones identified by geophysics could be intrusively studied.

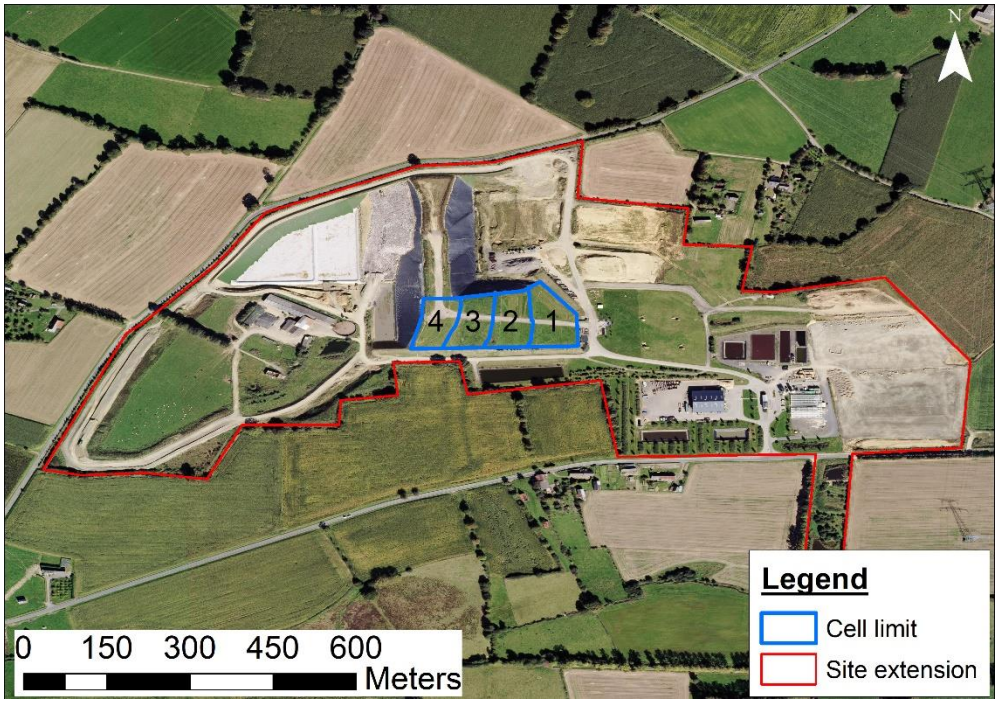

Figure 1: Overview of the landfill of Les Champs Jouault. In blue, the cells investigated during the pre-sampling geophysical survey.

Geophysical investigations during the second survey only focused on the area where intrusive investigations were planned, which is north of the road and crossing cells 1 to 3 (see Fig. 2).

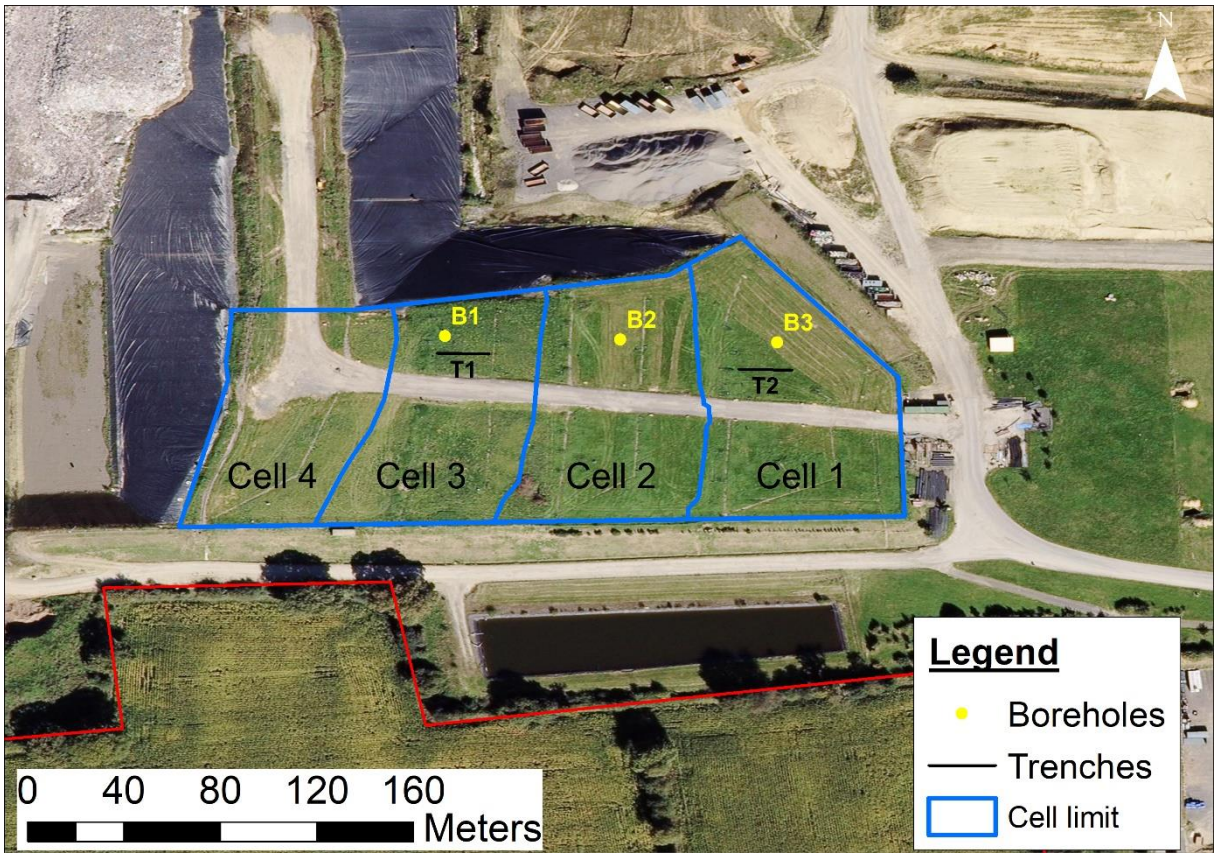

Figure 2: Sampling plan consisting in 3 boreholes and 2 trenches. The zone investigated during the second geophysical survey covers the area north of the road and crossing cells 1 to 3.

Geophysical investigations

In the following, all applied geophysical methods are listed with their expected main sensitivities on landfills. For a more detailed description of each geophysical method, please refer to the following report T1.3.1: Swot analysis of LF characterization methods.

In order to get a full areal coverage, the following mapping methods were used:

- **Electromagnetic (EM):** to reveal lateral extent of different waste composition or leachate content at several distinctive depths (mapping changes in electrical conductivity and magnetic susceptibility) – Fig. 3A.

More focused 2D surveys, providing detailed information about changes of physical properties with depth were done along distinct profiles including the following methods:

- **Electrical Resistivity Tomography (ERT) and Induced Polarization (IP)**: to discriminate different waste types, investigate changes in leachate content (measuring resistivity distribution) and to detect metallic scraps or zones of higher organic content (measuring chargeability distribution) – Fig. 3B.

- **Multichannel Analysis of Surface Waves (MASW):** to characterize the shear wave velocity structure of the subsurface indicating layers of different waste composition and the transition to the host material (measuring seismic velocities).
- **Capacitively-coupled resistivity:** to measure electrical properties of the subsoil without a galvanic contact such as in classical ERT surveys. The information provided by the method is the same as that provided by electrical resistivity tomography, but offers the advantage not to damage the geomembrane – Fig. 3C.

Finally, a last method giving punctual information about the geotechnical properties of the subsoil was applied:

- **Cone penetration test (CPT):** to gain information about landfill stratigraphy by measuring the penetration resistance of a cone pushed into the soil – Fig. 3D.

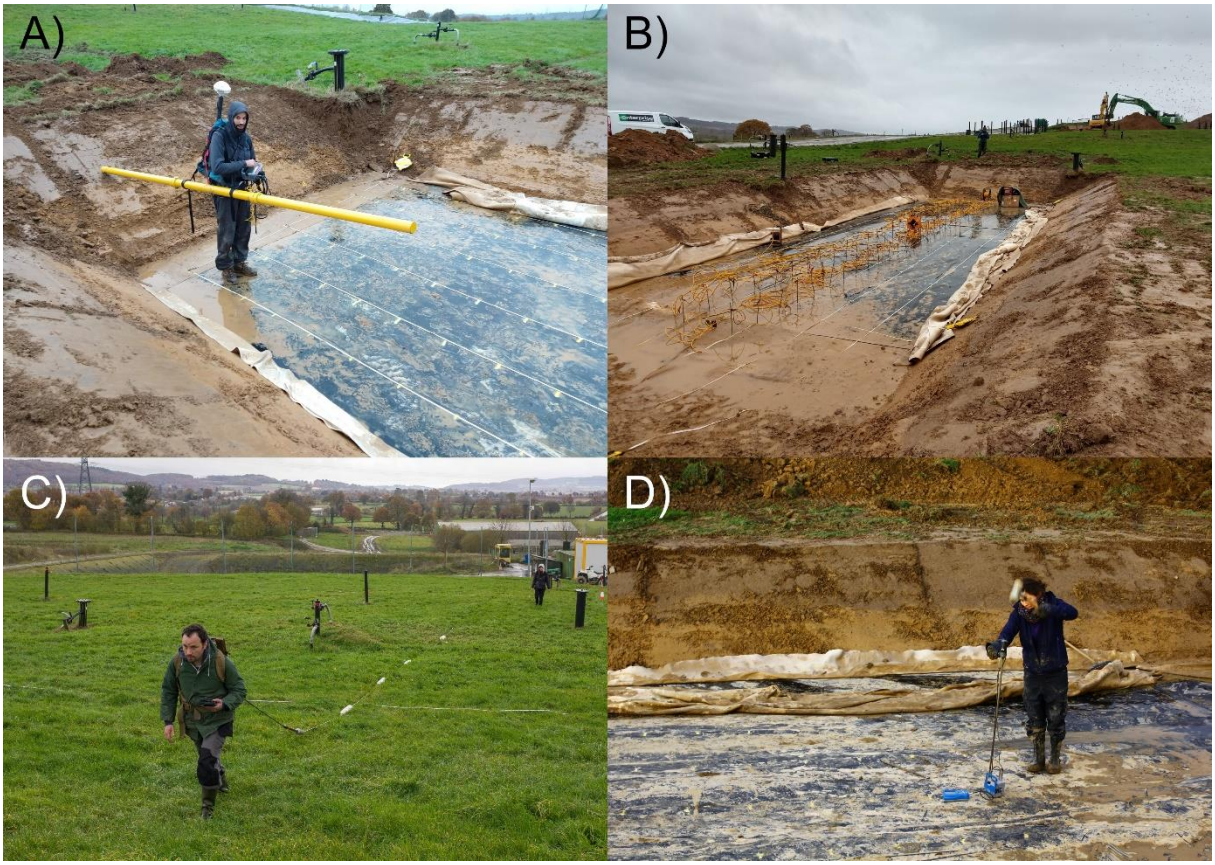

Figure 3: Acquisition of A) EM, B) ERT/IP, C) Capacitively-coupled resistivity and D) CPT

Measurement systems and parameters

In the following, the measurement parameters and areal coverage of each method are summarized in more detail.

The **electromagnetic** data was acquired using a conductivity meter model DUALEM-4. By attaching two different antennas sizes, mapping at four different depth levels could be achieved. These depths

were 0.5 m and 2.3 m for the shorter antenna and 1.8 m and 5.3 m for the longer antenna. Both quadrature (related to apparent conductivity) and in-phase (related to apparent magnetic susceptibility) components were recorded simultaneously for each antenna. In addition, a GPS sensor (no RTK) was connected to the system for positioning.

Two acquisitions were performed at different resolutions and coverage. The larger scale but lower resolution acquisition was done with the 4 m antenna covering the whole investigation area at a 4 m interline spacing before the removal of the cover layer (see purple dots in Fig. 4). This is a repetition of what was measured in November 2018 and was done with the perspective to quantify changes in conductivity connected to moisture/leachate content since the last survey. A second acquisition was done at a finer resolution over the location of the two trenches. For completion, this included crossing the trench location with the 2 m antenna before the removal of the cover layer. After the removal of the cover layer, a fine grid with interline spacing of 0.8 m in cell 1 and 1 m in cell 3 was measured with the 2 m and the 4 m antenna directly on the HDPE-membrane (see yellow dots in Fig. 4). These finer resolution surveys over the trenches were done in order to allow a detailed correlation analysis between the EM data and the ground truth data from trenching.

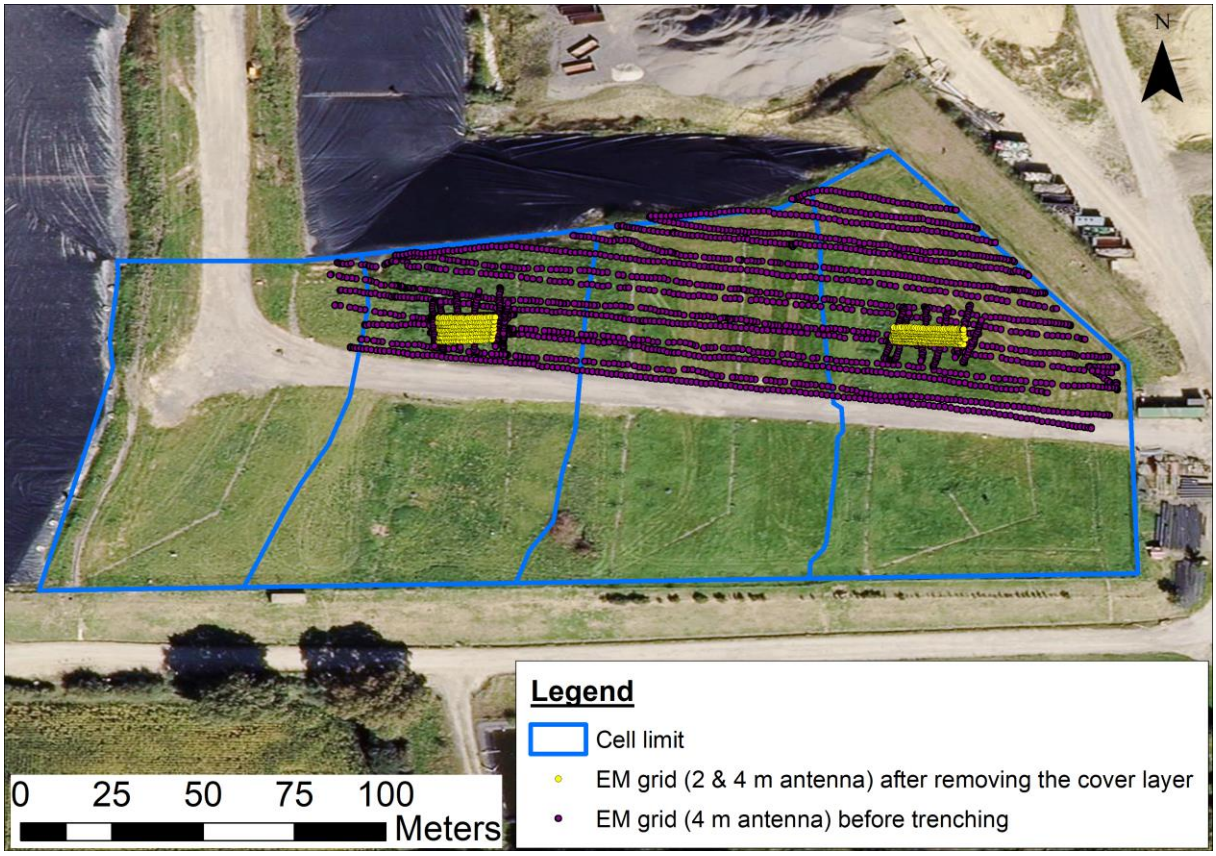

Figure 4: Extent of the EM mapping with the 4m antenna before (purple dots) and after (yellow dots) the removal of the cover layer

Electrical resistivity tomography (ERT) and time-domain induced polarization (TDIP or IP) data were acquired with an ABEM Terrameter LS system. Five profiles were deployed at the location of the trenches after the excavation of the cover layer (see Fig. 5). Each profile contained 32 stainless steel electrodes, which were planted though the liner. In cell 1 (Profiles 1 to 4), the electrode spacing was 0.45 m and the spacing between each profile was 0.8 m. In cell 3 (Profile 5), the electrode spacing was

reduced to 0.35 m. For the data acquisition, we used a gradient configuration with a 's' factor equals to 8 (Dahlin and Zhou, 2006). Electrical current injection was setup to 2 s (delay of 0.8 s and acquisition of 1.2 s) and voltage decay was measured for 1.86 s after current shut down. Measurements were repeated twice to estimate the repetition error. Reciprocal resistivity measurements were also collected for each profile to assess the quality of data.

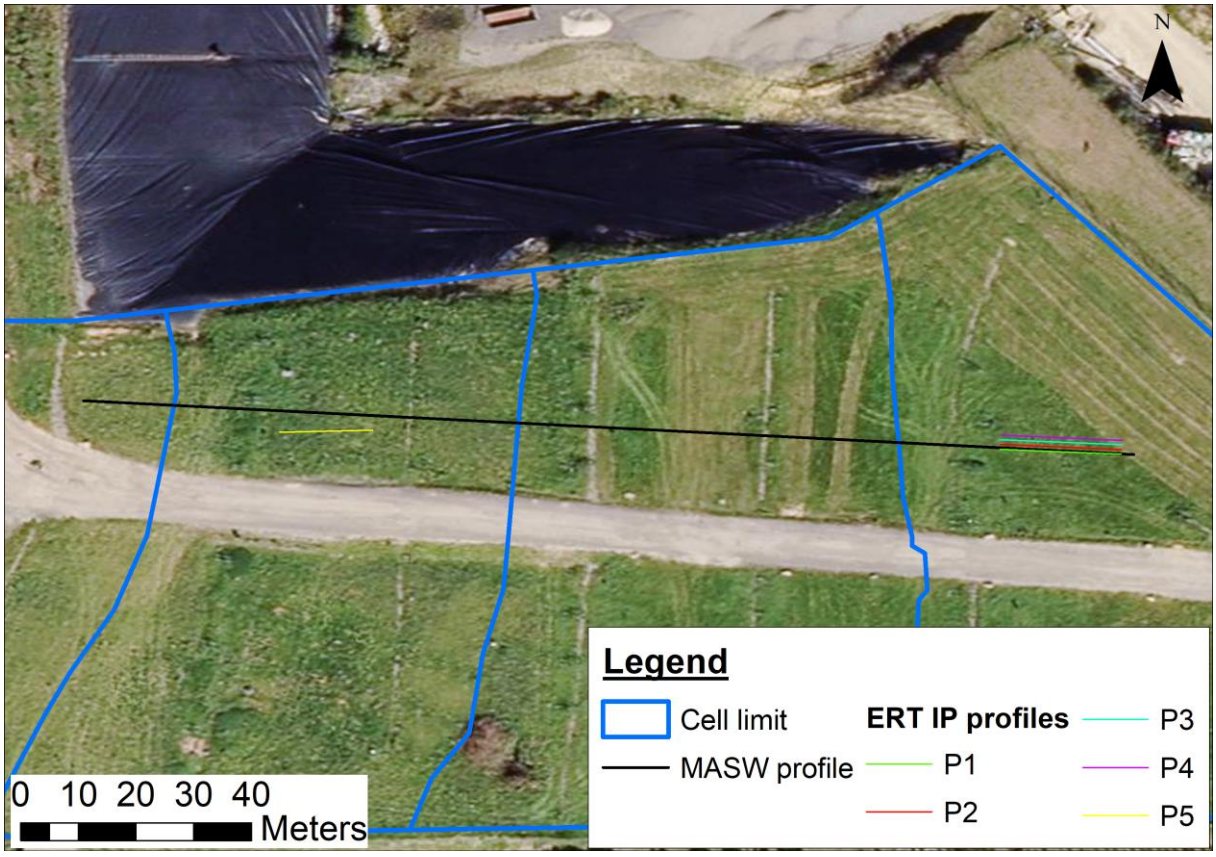

Figure 5: Location of the ERT/IP profiles after the cover layer removal. The MASW profile was measured before the cover layer removal.

One **MASW** profile was measured crossing all three cells and measuring over the trenches before the removal of the cover layer (see Fig. 6). The data was acquired using a Geometrics Geode Seismograph, utilising a towed geophone streamer deployed from a wheelbarrow. The streamer consisted of 24 vertical geophones (4.5 Hz natural frequency), mounted on ground-coupled base plates at 1 m centres and connected by woven Kevlar reinforced webbing. A 5 kg sledgehammer and ground-coupled striking plate was used as a seismic energy source, with the source located 2 m ahead of the geophone streamer. In order to increase the signal to noise ratio (SnR), a total of three hammer blows were stacked at each shot location.

The **capacitively-coupled resistivity** was acquired with a Geometrics OhmMapper consisting in one ungrounded dipole transmitter and three receivers. The transmitter and receivers have a dipole-dipole configuration where the transmitter and receivers were separated by a distance equal to N (=0.02,0.5,1) times the dipole length fixed at 5 m. Several profiles were acquired in the same location of the EM grid before trenching (Fig. 4). However, due to the large conductivity in some areas, the three receivers were not continuously detecting the transmitted signal, hence the depth of investigation was very shallow. To show this we inverted a profile using RES2DINV and two receivers (N=0.5 and 1), see Fig. 6. Despite the short amount of points, we can see a rough change in the resistivity values corresponding to the interface between the cover layer and the upper limit of the waste. The very large values observed in this inverted model might correspond to a poor coupling between the antennas and the rough surface of the soil.

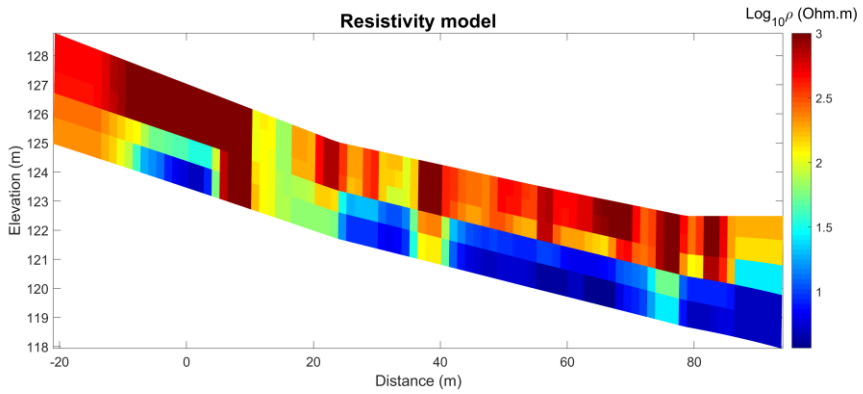

Figure 6: Inverted model of one capacitively-coupled resistivity profile located in the southernmost part of the EM grid with a W-E orientation. RMS error of 5.7.

The intrusive **Cone Penetrometer Test** (**CPT)** data was acquired with a PANDA system. This system consists of a cone attached to a metallic rod, which is hammered into the ground. For each hammer blow, the system measures the penetration depth and the impact velocity of the hammer. This allows obtaining one-dimensional profiles of change in penetration resistance with depth, which relates to changes in ground stiffness with depth.
In total, five CPT measurements were acquired at different locations. One measurement was done through the cover layer in order to detect layering within the cover layer. The other four CPT measurements were done within the trenches at positions on the ERT lines. Three of those were done in the eastern and one in the western trench (see arrows in Figs. 7 and 8).

Geophysical processing and results

The processing of data and results of each geophysical method are described in the following section. A conclusion at the end of the section discusses the overall interpretation with respect to the landfill characterization.

ERT and IP results

Data collected were first filtered by removing all measurements characterized by a repetition error on the measured resistance larger than 5%. Then in order to weight the data in the inversion process, individual data errors were calculated using the reciprocal data collected during the acquisition. The weighted data were inverted with BERT (Günther et al., 2006; Rücker et al., 2006) using a robust constraint on the data and a smoothness constraint on the model. Models obtained with BERT satisfy the error weighted chi-square, $\chi^2 = 1$ meaning that the data are fitted to their error level.

We provide in Fig. 7 the resistivity and chargeability models obtained for profile 1 in cell 1. The models obtained for the other profiles being relatively similar, they are shown in Annex. Globally, the resistivity are very low (< 30 Ohm.m). We nevertheless distinguish a more resistive layer close to the surface, which can be attributed to the presence of clay. Interestingly, this layer seems to be a bit thicker westward. Underneath this layer, very low resistivity and high chargeability are observed. This particular geoelectrical signature is typical of MSW and ISW. In the bottom right part of the provided models, we observe a slight increase of resistivity and a decrease if chargeability. This zone of the models is more difficult to interpret given the loss of sensitivity with depth. One possible explanation is a soil filling between different waste layers.

As seen in Fig. 9, the resistivity values obtained in cell 3 are generally higher than in cell 1, especially on the western part of the profile. During the installation of the electrodes, it was obvious that there were more voids below the liner in the upper part of the profile, which may partly explain the higher electrical resistivity observed. The presence of rainwater infiltrating cell 1 due to electrode perforating the liner might also partially explain lower resistivity values. Nevertheless, we can detect two main layers in cell 3, one probably related to the clay layer below the liner and one below related to the MSW and ISW.

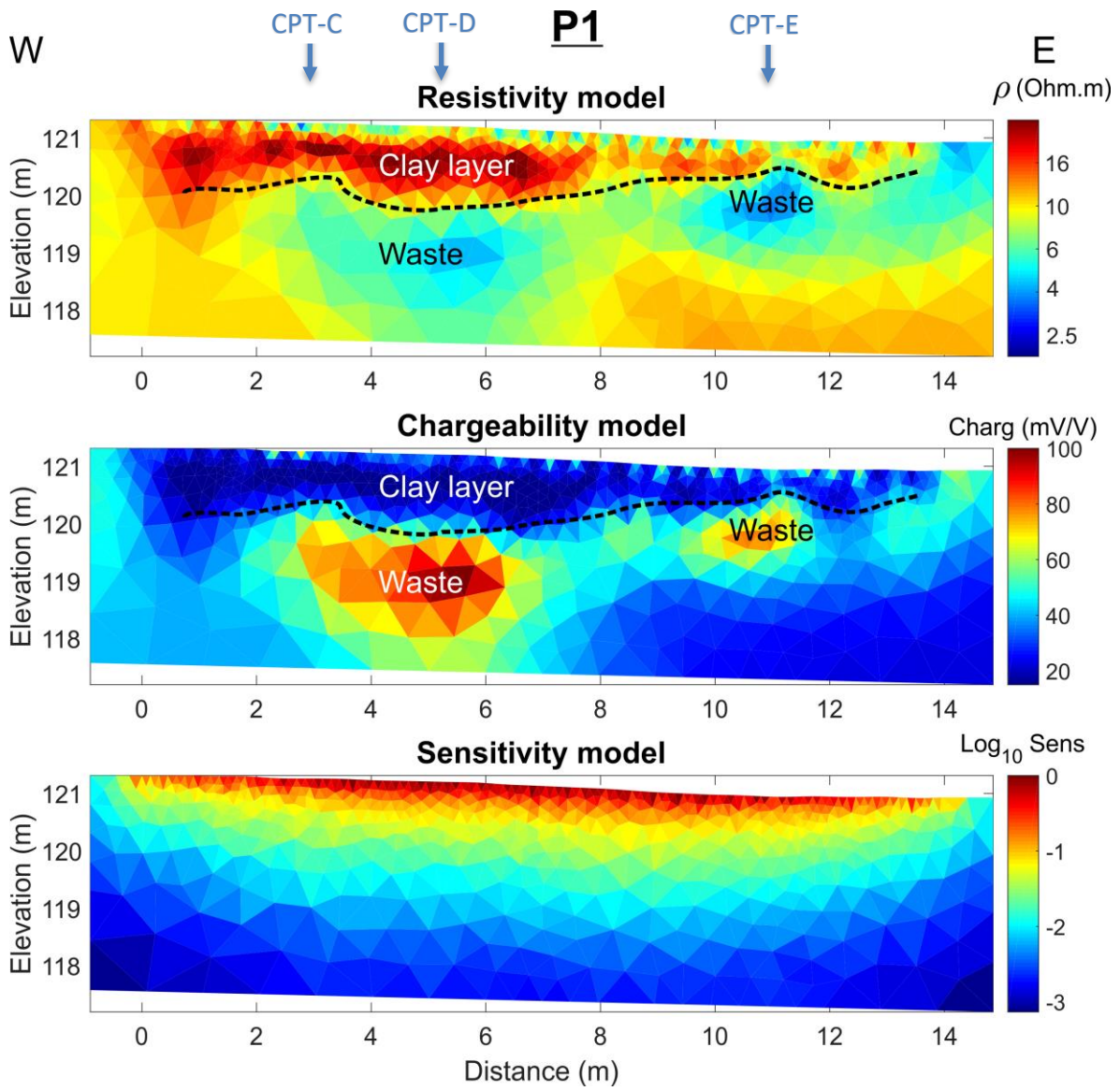

Figure 7: Electrical resistivity and chargeability models obtained in the first profile in cell 1. Positions of the CPT measurements are indicated with blue arrows.

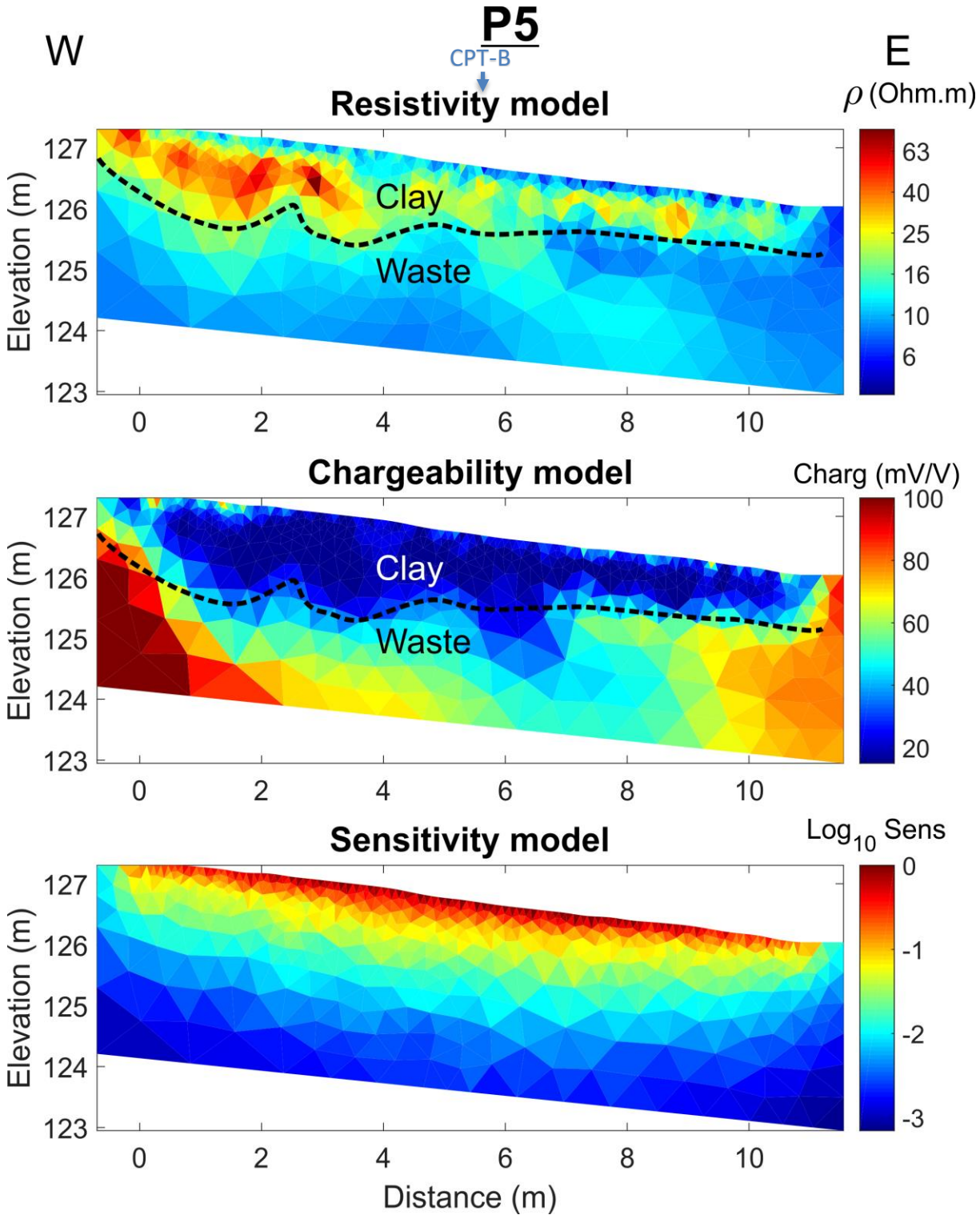

Figure 8: Electrical resistivity and chargeability models obtained in the fifth profile in cell 3. The position of the CPT measurement is indicated with a blue arrow.

EM results

In order to produce maps of the EM data, all individual data points were interpolated with IDW. The quadrature-phase component of the induced magnetic field can be related to the electrical conductivity and the in-phase component to the magnetic susceptibility (e.g. Dumont et al., 2017). The data is sensitive to different depths depending on the antenna used, either 2 m or 4 m antenna, and the orientation of the coils. This allowed us to derive four maps corresponding to 0.5 m, 1.8 m, 2.3 m and 5.3 m depths below the surface. However, these depths are indicative only. Due to the integrative nature of the EM measurements, they refer to depths of maximum sensitivity, which are influenced by the vertical and lateral distribution of conductivity in the vicinity of the sensor. In the following, we discuss only the conductivity maps only since the magnetic susceptibility data provided no new relevant information.

The maps in Fig. 9 compare the derived conductivity measured on the first survey in November 2018 (A to D) to the new data acquired before the removal of the cover layer (E to H). The maps from the top to bottom correspond to the different investigation depths. It has to be noted that the broader looking stripe pattern in the new data (E to H) is caused by the larger interline spacing during the recent survey and is not related to any changes in the cover layer or landfill material.

Overall, the conductivity distribution of both surveys show a very similar pattern. However, some parts, especially in cell 2 and 3, show a decrease in conductivity since November 2018. In addition, the high conductivity anomaly seen immediately to the North of the road in cell number 3 is not visible anymore (compare 10b to 10f). This could be linked to a decreased leachate content since November 2018.

Figure 10 displays the conductivity data measured in the western (10A) and the eastern (10B) trench after the removal of the cover layer. For both trenches, the conductivities corresponding to the shallowest depth at 0.5 m are significantly lower than the ones corresponding to deeper depths. This is in accordance with the ERT data, which show a high resistivity layer just beneath the membrane (see Fig. 7 and 8). At the following depths, a conductivity decrease towards East is seen in both trenches. As shown in the ERT data, this is probably associated with a thinning of the higher resistive clay layer. The conductivity decrease towards East at the deepest depth in the eastern trench could be associated with a change in waste material (e.g. more inert waste). Overall, the conductivities measured in the western trench are higher. This is again in accordance with the generally lower resistivities seen in the ERT data. However, the thicker clay layer indicated by the chargeability data (see Figs. 7 and 8) would normally be expected to cause lower conductivities. It can therefore be assumed that the leachate content at the location of the western trench (cell 3) is higher than at the eastern trench (cell 1).

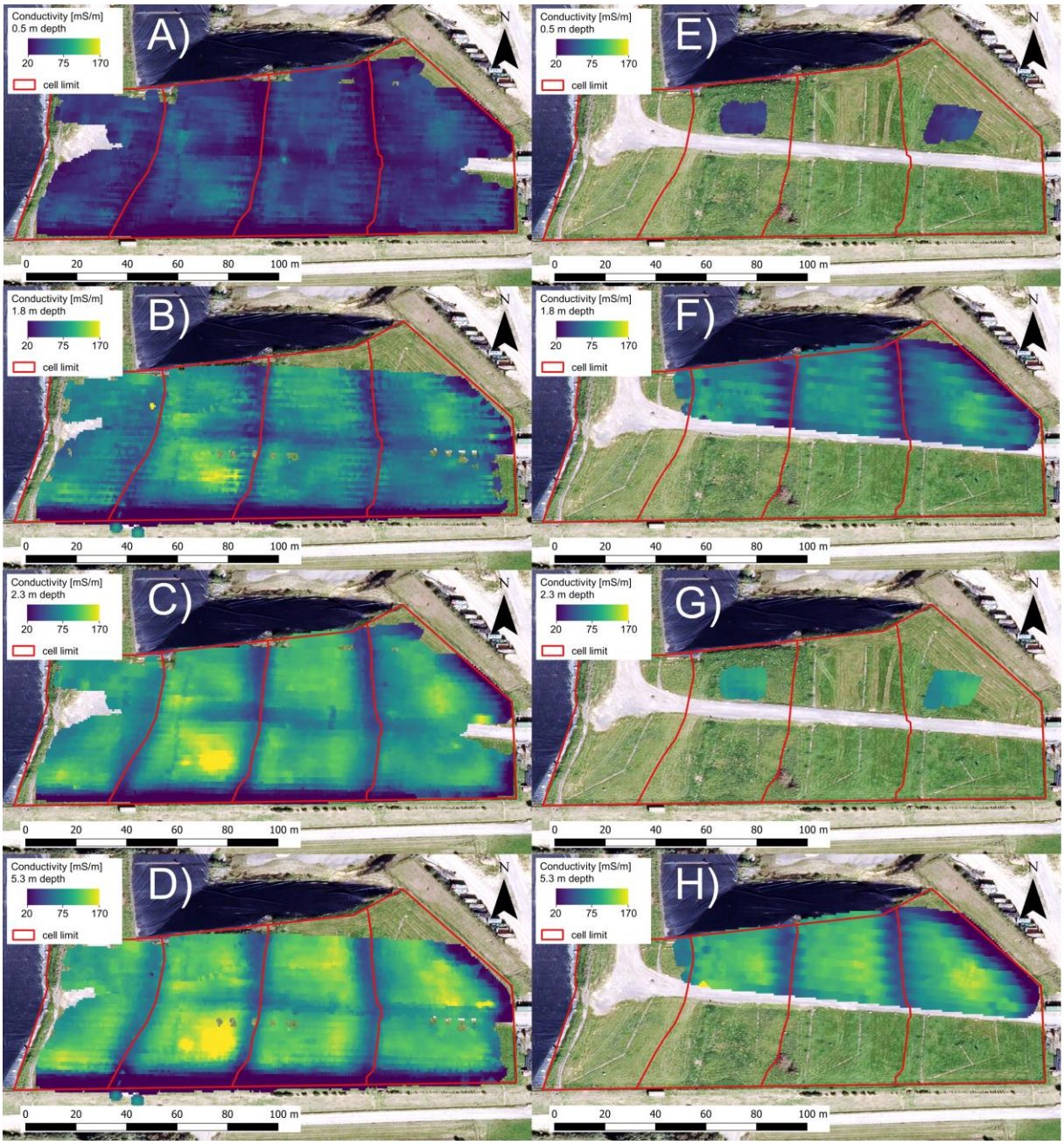

Figure 9: Electrical- conductivity maps derived from the measured quadrature-phase data. Investigation depths are from top figure to bottom: 0.5 m, 1.8 m, 2.3 m and 5.3 m. A to D display the data acquired in November 2018. E to H display the data acquired before the removal of the cover layer in November 2019.

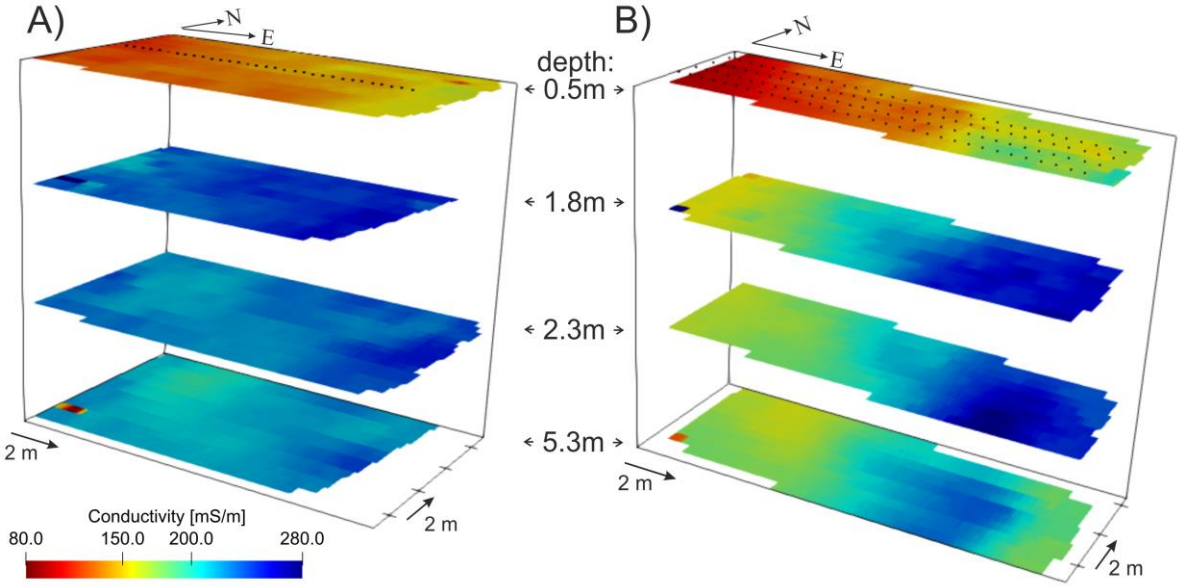

Figure 10: Depth slices showing the conductivities measured in the western (A) and the eastern trench. The black dots indicate the position of the ERT profiles.

MASW results

The MASW data was processed in the same way as the data from the first geophysical survey using the SurfSEIS software (Kansas Geological Survey (KGS)). Each shot record was transformed to calculate the phase velocity-frequency distribution, also known as a dispersion curve and the fundamental mode of each dispersion curve was then picked. From the dispersion curves two methodologies (approximate and inversion) were used to construct shear wave velocity profiles (for more details see Deliverable I2.2.2). The results of each of these methods are displayed in Figure 11 below.

Irrespective of the modelling procedure applied, the velocity distribution shows a very similar pattern to what was found during the survey in November 2018 (see Deliverable I2.2.2). In general, the velocity distribution of the new survey appears to be more homogeneous. However, this is caused by the larger spacing of 5 m between the show locations and doesn't reflect any property changes since November 2018.

The waste material is characterised by very low shear wave velocities of less than 120 m.s ^{1}. Below the waste, a significant increase in the velocity indicates the transition to the host material having velocities > 230 m.s^{-1}. The corresponding interpreted bottom of the waste is shown as a white dashed line in Figure 11. This indicates the maximum thickness of waste expected across the site, which is 17m beneath the surface (2m of cover materials plus a maximum of 15m of waste).

As seen in November 2018, very low velocities are noted to extend up to the surface of Cell 3. This suggests higher moisture content in this cell (compared to the other cells) and would correspond to what was observed with the EM measurements.

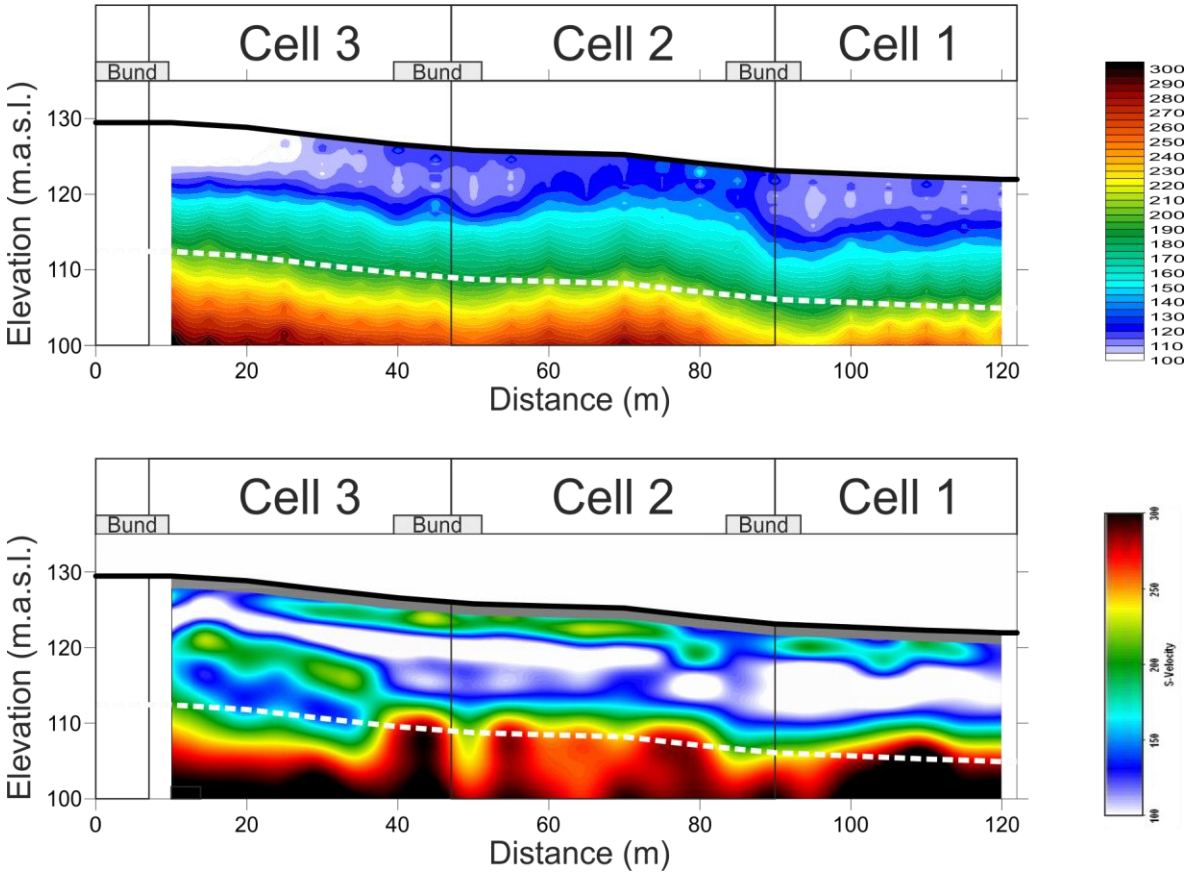

Figure 11: 2D shear wave velocity profiles constructed for the MASW line acquired across the two trench locations (W-E oriented, see Figure 6). Upper-Approximated velocity profile assuming an investigation depth equal to 1/3 of the wavelength of the Rayleigh wave. Lower-Inverted velocity profile derived using a 10 layer starting model and varying thickness of layers. Dashed white line indicates the maximum thickness of waste expected at site (17m below the surface).

CPT results

All CPT measurement results are displayed in Figure 12. Figure 12A displays the one-dimensional depth-profile through the cover layer acquired south of the eastern trench. Figures 12C to E display the CPT results acquired at positions on the cental ERT line in the trench of cell 1. Figure 12B presents results in the center of the ERT line in the trench of cell 3. They correspond to a one-dimensional profile through the waste material directly beneath the membrane (see Figs. 7 and 8 for positioning on the ERT line).

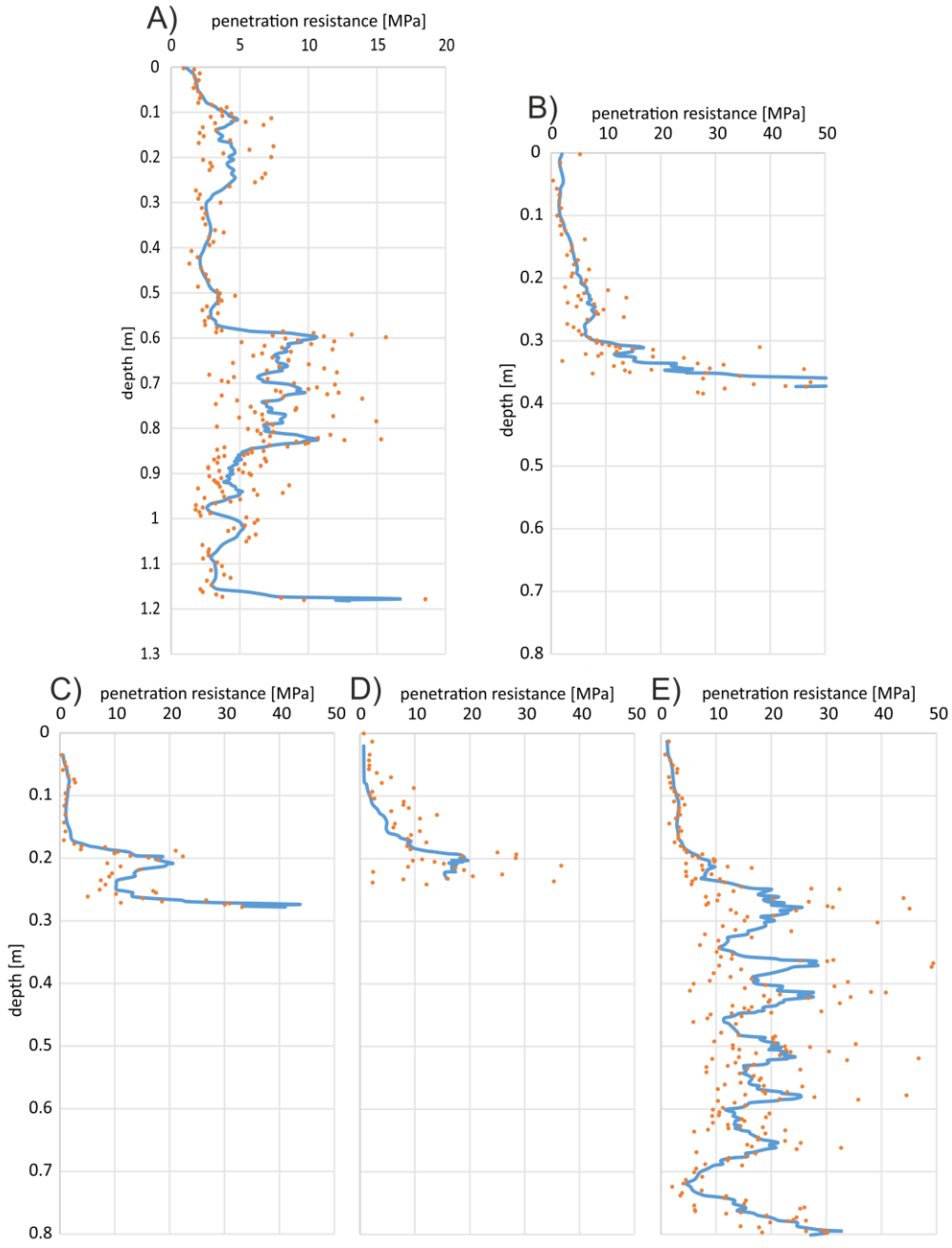

Figure 12: CPT results. A) 1D-depth-profile through the cover layer south of the eastern trench. B) 1D-profile through the waste material beneath the membrane in the western trench. C to E) 1D-profiles acquired in the eastern trench (see Figures 7 and 8 for locations along the ERT profiles).

The 1D-profile in Figure 12A shows a distinct increase in penetration resistance at about 0.6 m depth. This might correspond to the boundary between the arable cover and the loam layer within the cover layer.

All depth profiles within the trenches show a layer of comparably low resistance on top. This layer is in the western trench about 45 cm, which is thicker than in the eastern trench where it reaches a thickness of 20 to 25 cm. It might correspond to a clayey or sandy soil layer, which was placed at the top of the cell to protect the HDPE-membrane. On the ERT profiles, it corresponds to the very thin layer of low resistivities seen along the top of the higher resistive layer interpreted as “clay layer” (see Figs. 7 and 8). The profiles in Figure 12B to D, stop at shallow depth where the metal rod was stuck on hard items. Thus, this indicates that the layer interpreted as “clay layer” on the ERT profiles might contain relatively big, blocky items (e.g. mixed inert material). Only the easternmost measurement displayed in Figure 12E could penetrate deeper until 0.8 m depth where the rod was stuck. This is in accordance with the ERT line in Figure 7, which shows that the clay-inert layer is very thin at the location of CPT-E. From 0.2 to 0.8 m, the penetration resistance is quite scattered and shows that this layer is certainly inhomogeneous.

Conclusions

The second geophysical survey in LCJ provides a baseline to compare with the invasive sampling results performed on the trenches and boreholes. It also allowed to refine our understanding of the northern part of the cells 1 to 3 where the drillings and trenches were conducted. ERT/IP data allowed to identify different layers within the upper part of cells 1 and 3 that were attributed to a clay layer below the liner and the waste body respectively.

The EM data, in accordance with the ERT data, is indicating a thinning of the clay layer towards East in both trenches. In addition, both the EM and the ERT data, indicate a potentially higher leachate content in cell 3 compared to the other cells. The MASW data shows a very similar pattern of what was seen on the previous survey highlighting the interface between the waste and the natural ground by a clear increase in shear wave velocity.

As a next step, the detailed analysis correlating the geophysical measurements with the available ground truth data from the drilling and trenching should allow us to provide a more detailed interpretation.

References

Dahlin, T., Zhou, B. 2006. Multiple-gradient array measurements for multichannel 2D resistivity imaging. *Near Surface Geophysics*, 4: 113-23.

Dumont, G., Robert, T., Marck, N., Nguyen, F. 2017. Assessment of multiple geophysical techniques for the characterization of municipal waste deposit sites. *Journal of Applied Geophysics*, 145: 74-83.

Günther, T., Rücker, C., Spitzer, K. 2006. Three-dimensional modelling and inversion of DC resistivity data incorporating topography—II. Inversion. *Geophysical Journal International*, 166: 506-17.

Rücker, C., Günther, T., Spitzer, K. 2006. Three-dimensional modeling and inversion of DC resistivity data incorporating topography—Part I: Modeling, *Geophysical Journal International*, 166: 495-505.

Contact

Feel free to contact us.

Local contact details:

BELGIUM	ATRASOL	renaud.derijdt@atrasol.eu
	Cleantech Flanders / VITO	alain.ducheyne@vito.be
	OVAM	ewille@ovam.be
	SPAQuE	c.neculau@spaque.be
	Université de Liège	f.nguyen@ulg.ac.be
FRANCE	SAS Les Champs Jouault	champsjouault@gmail.com
GERMANY	BAV	pbv@bavmail.de
THE UK	NERC	jecha@bgs.ac.uk

Coordination office:

BELGIUM	SPAQuE Boulevard Maurice Destenay, 13 4000 Liège	c.neculau@spaque.be